MODELLING AND TESTING OF SATURATED CORE FAULT CURRENT LIMITER

David KLAUS
ASG Power Systems - UK
klaus.david@as-g.it

Antonio MORANDI
University of Bologna – Italy
antonio.morandi@unibo.ita

Antonio PELLECCHIA
ASG Superconductors - Italy
pellecchia.antonio@as-g.it

Gianni GRASSO
ASG Superconductors - Italy
grasso.gianni@as-g.it

ABSTRACT

A fault current limiter (FCL) is a nonlinear device with negligible impedance under normal conditions which is able to switch to a high impedance state as soon as the current passing through it exceeds a given threshold. Among the various FCL topologies, saturated core fault current limiters have recently reached the demonstration phase in medium to high-voltage networks. ASG Power Systems has manufactured and tested a 36kV rated saturated core type fault current limiter (FCL). The Paper presents a sophisticated coupled-circuit model of the limiter and compares the model results with the results of full-scale testing of the limiter.

INTRODUCTION

Fault current limiters will become important components for future electric power grids with increased levels of interconnection and increased numbers of distributed generators. FCLs will provide improved stability and power quality during normal conditions as well as reduced vulnerability and reduced voltage disturbance during faults [2]-[3]. Among the various FCL technologies, saturated core fault current limiters have reached the demonstration phase. Several prototypes have in fact been developed based on first generation high temperature superconductors and successfully submitted to live test in medium to high-voltage networks [4]-[10].

A saturated core type fault current limiter rated 36kV; 800A has been recently developed and submitted to full-scale laboratory testing comprising thermal, short-circuit, high-voltage withstand and partial discharge tests.

Description of the FCL

The device comprises an oil-filled reactor tank containing six laminated, vertically mounted steel cores. Around each core is a winding of continuously transposed copper (CTC) conductor. Adjacent pairs of cores have their windings connected in series, each pair of windings carrying the AC current of one phase of the network into which the FCL is connected. A schematic illustration of the FCL construction is shown in Fig. 1 (the windings of one phase only are shown).

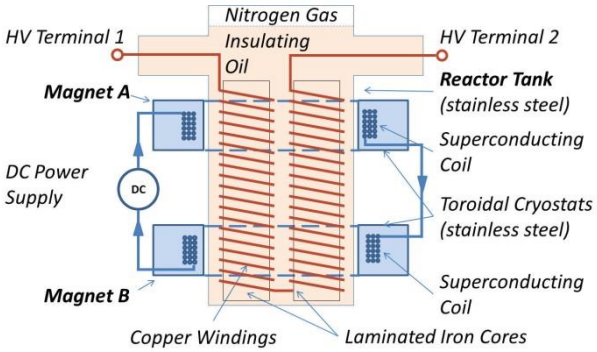

Fig. 1. Schematic Diagram of the FCL

The reactor tank cores are magnetically saturated by means of two magnesium diboride (MgB_2) solenoids, labelled Magnet A and Magnet B.

Parameter	Requirement
Rated voltage	36 kV
Line frequency	50 Hz
Line voltage	33 kV
Lightning impulse withstand level	170 kV; 1.2/50 µs
Power frequency withstand level	70 kV/1 minute
Max voltage drop at I_n	600 V_{rms}
Rated normal current I_n	800 A
Maximum normal current/time	1400 A_{rms} /15 minutes
Peak fault current	20.9 kA
Symmetrical fault current	7.8 kA_{rms}
Limited peak fault current	13.0 kA
Limited sym. fault current	4.8 kA_{rms}
Fault duration	3 seconds
Overall size: Total footprint including cooling and supervisory control	54m^2 x 3.6m height
Overall weight	45 tonnes

TABLE I: FCL SPECIFICATION

Table I shows the specification to which the FCL has been designed.

CURRENT LIMITING

The FCL presents low impedance to the passage of load

current when the six AC winding cores are saturated. At higher currents, the FCL impedance rises, autonomously, without any current measurement, decision making, or issuing of an actuation command – the impedance rise at high current is implicit in the physical design – and is due to the change of the magnetic state of the cores. The network current flows through the two series-connected AC coils, which are wound on the laminated steel cores (Fig. 1). These are saturated by flux produced by magnets A and B. The flux produced by the AC current opposes the saturating flux in one of the coils, and augments the saturating flux in the other. If the opposing flux produced by the AC current is sufficient to de-saturate the core, the inductance of that coil rises to that of an iron-cored reactor. Thus each half-cycle of the fault current causes the de-saturation of one of the two AC coil cores, raising the impedance of that coil. The rise in impedance is sufficient to reduce the AC current magnitude, providing the current limiting functionality.

COOLING SYSTEM

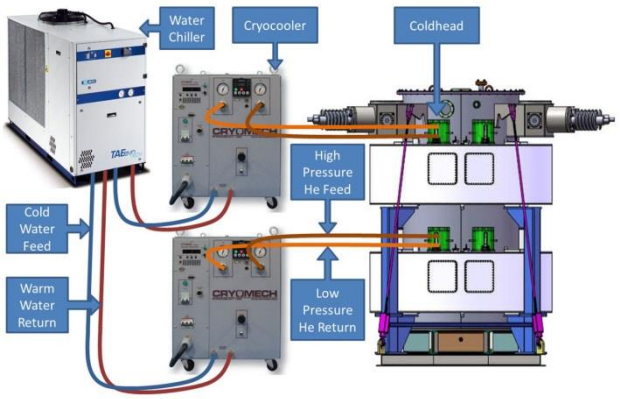

Fig. 2. Magnet cooling system

Each of the two superconducting magnets is fitted with four Gifford-McMahon coldheads, connected inside the vacuum vessel to the epoxy encapsulated MgB_2 coils by means of copper cooling strips. Helium gas at around 20 atm. is circulated between each coldhead and its compressor and each pair of compressors is cooled by a single water chiller, as shown in Fig. 2. The whole system comprises four chillers and eight compressors and coldheads. The total power consumption (400V, 3-phase) is around 100kW.

Arrangement at site

The FCL comprises a GRP enclosure (approx. 3,1 x 4.6 x 4.6m) for the AC reactor tank and magnets and two 6m (half shipping container) enclosures, one for the water chillers and the other for the helium compressors, PLC and SCADA systems, DC supply and electrical interface for connection to the network operator's control system. The reactor tank is mounted on a plinth inside an oil bund with 6,000 litre capacity and the two auxiliary enclosures are on a concrete plinth alongside, as shown in Fig. 3.

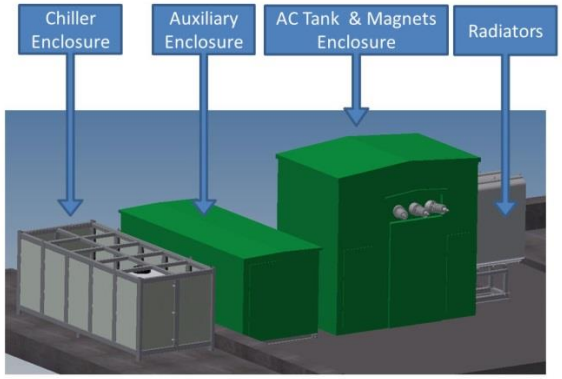

Fig. 3. Arrangement at site

NUMERICAL MODEL

A numerical model [11] of the FCL was developed and coupled with the circuit model of the power network, to investigate the performance of the FCL and its interaction with the power grid.

Fig. 4 shows the geometrical model of the FCL on which the numerical model is based. Only the main components with significant electrical conductivity and the saturable steel cores are incuded.

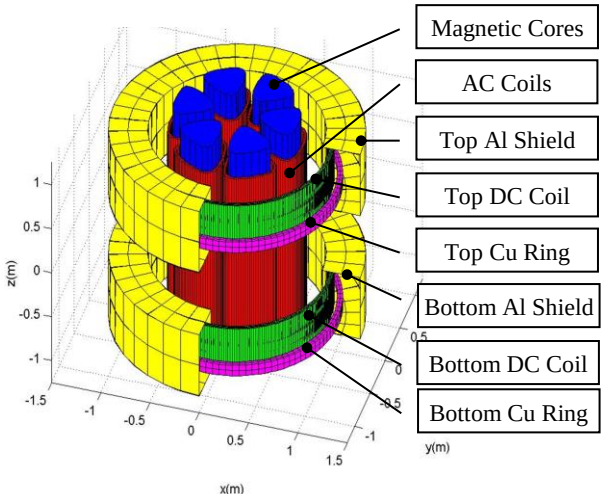

Fig. 4. 3D view of the FCL geometry.

The superconducting magnets comprise epoxy encapsulated multi-filament MgB_2 wire windings (green) of 3816 turns arranged in 30 layers, cooled by means of copper rings (purple) and shielded from radiated heating by aluminium shields (yellow). The AC reactor tank contains the six rounded triangular section steel cores (blue) and the six AC windings (red).

Details of the superconducting magnet design are shown in Table 2.

Cross section of the conductor	1.2×3 mm^2
Coil Inner radius	903 mm
Coil Outer radius	946 mm
Height	410 mm
Number of turns	3816
Number of layers	30
Total length of conductor (one coil)	22.1 km
Axial separation of the coils (centre to centre)	1400 mm
Nominal current, I_n	97 A
Operating temperature	16 K
Maximum field on the conductor at I_n, T	1T
Inner radius of the cryostat	841 mm
Outer radius of the cryostat	1097 mm
Height of the cryostat	785 mm

TABLE II: MgB2 Wire and winding details

The two superconducting magnets are energised at 97A by means of a single DC power supply as shown in Fig. 5. The voltage taps in the middle of each of the two coils are for quench detection purposes. A dump resistor of 2Ω is connected to each of the two coils to allow fast discharge if a quench occurs.

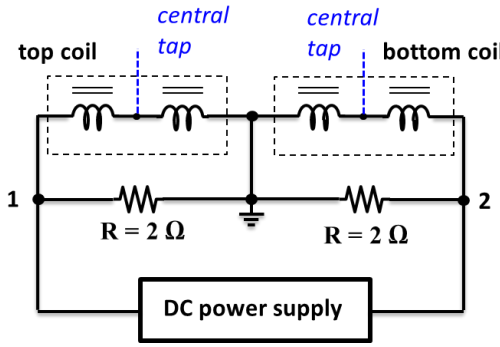

Fig. 5. DC power supply connection

The inductance of the DC coils, as seen from terminals 1 and 2 of Fig 3, changes from 220H in case of zero current to about 84H when the current reaches the nominal value I_n = 97A. The overall energy of the coils at the nominal current is 395kJ. The total charging time, starting from zero current up to the nominal value I_n, is less than 30 minutes.

Combined model of power grid and FCL

Fig. 6 shows the circuit model and Table III shows the values of the circuit element data used for the simulations. The load impedance is set to consume 45 MVA at 0.98 power factor.

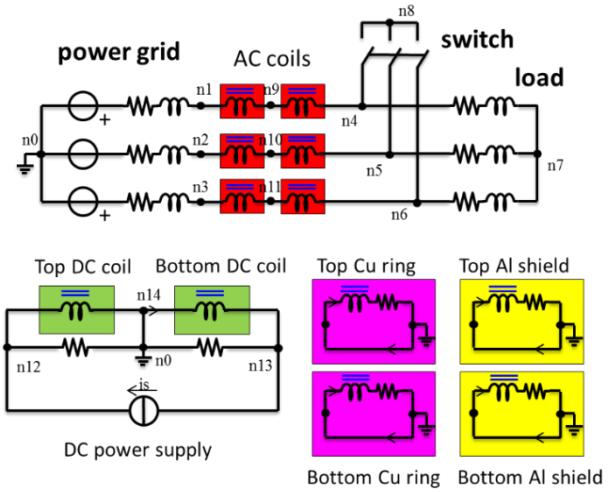

Fig. 6. Circuit model of power grid and FCL device

Power grid	
RMS Voltage	33 kV
Resistance	0.13 Ω
Reactance	2.47 Ω
Load	
Resistance	104.5 kΩ
Reactance	21.2 kΩ

TABLE III: CIRCUIT DATA

The AC coils of the FCL and the two DC superconducting magnet coils are modelled as inductances coupled via the ferromagnetic cores. Each of the AC coils has a resistance of 8.35 mΩ which is included in the model although it is not shown in Fig. 6.

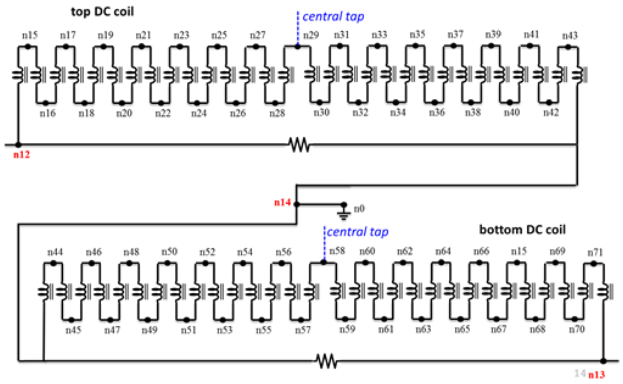

Fig. 7. Circuit model of the two MgB2 coils.

One of the goals of the numerical model is the calculation of the voltage appearing across the DC coils during a fault. To achieve this each of the 30 layers of each DC coil is modelled as a separate inductor, as shown in Fig. 7 with all the layers of one winding connected in series. The aluminium radiation shields and the copper rings for cooling the DC coils (see Fig. 4) are also included in the model, divided into finite numbers of loops, each with

azimuthal current. Non-axisymmetric distributions of current density in the shields and the rings are not taken into account. Each of the loops acts as a short circuited resistive inductor coupled with the AC coils, the DC coils and all other loops and hence each is modelled as a coupled inductor. For simplicity, only one loop is shown for the shields and the rings of the upper and the lower DC coils in Fig. 6. The stainless steel cryostat and the oil tank are not taken into account as they do not affect the results significantly. Values of the self/mutual inductance coefficients of the FCL circuit model are obtained by real time finite element modelling of the device (based on the geometrical model of Fig. 4) at each time step of the circuit simulation.

The node voltage method is used for solving the circuit of Fig. 6 using an implicit Euler scheme for iterative calculation of the numerical solution. This is described in full in [11].

RESULTS AND DISCUSSION

Fig. 8 shows the fault currents in the three phases of the network during a three phase fault of 200ms. Fig. 9 shows the phase voltage drops in the three phases of the FCL device during the fault.

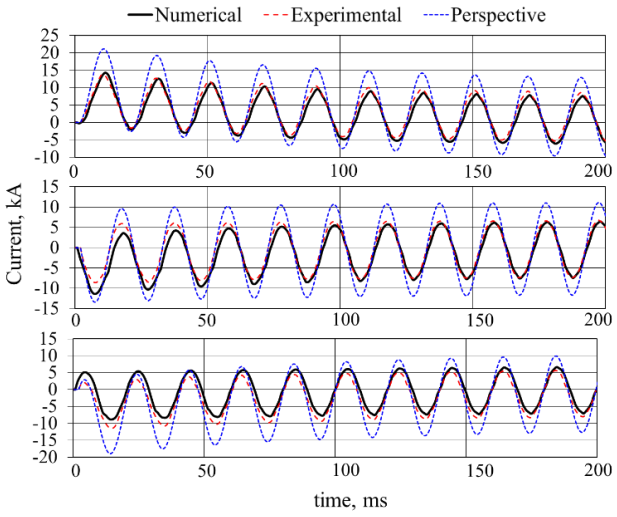

Fig. 8. Fault currents in the three phases of the FCL. The prospective fault current is also shown.

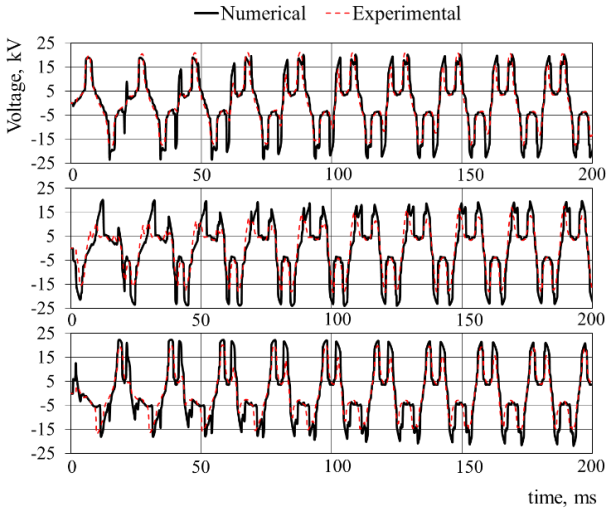

Fig. 9 Voltage drops in the three phases of the FCL

Both calculated and measured data are shown in Figs. 8 and 9. Experimental data were measured during the short circuit test performed at the IPH laboratory in Berlin. The measured prospective (unlimited) fault current is also shown in Fig 8 for comparison. It can be seen that the FCL's current limiting performance requirement has been achieved: the impedance increase during the fault prevents the fault currents from rising to the full level. The fault is limited by about 40 %. Furthermore, good qualitative and quantitative agreement between measured and calculated results can be seen from Figs. 8 and 9. The model is able to reproduce the relevant physics of the device and can be used for accurate predictions. As the model is sufficiently general in nature, it allows variations on the FCL design to be evaluated. The modelling methodology developed will be applicable to a wide range of FCL voltage and current ratings and current limiting capacities.

The total voltage induced across the DC coil (from the input to grounded output terminal) reached a relatively small value during the fault. Nevertheless, substantial voltages appear distributed within the coil. Fig. 10 shows the calculated voltage in one of the DC coils during the fault.

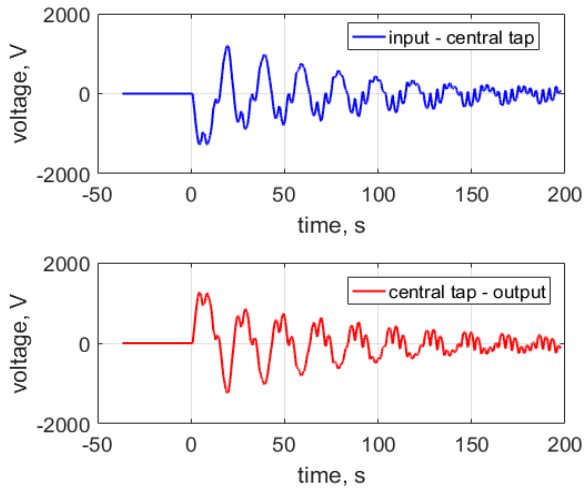

Fig. 10 Induced voltage in magnet winding

A voltage peak of about 1.3 kV is reached from the input terminal to the central tap. About the same voltage, but with reverse polarity, is reached form the central tap to the grounded output terminal. These values of voltage are within the designed insulation level of the DC coil.

CONCLUSION

Closed-core FCLs described in [1], [10] and [4] are bulky and insulation of the high voltage parts is difficult, whilst maintaining good coupling between the AC and DC coils. The open core solution described here and in [9] provides a highly compact and easily uprated device, as all of the high-voltage parts are contained in a single oil-filled enclosure. This approach also provides easy access for maintenance of the cryogenic systems.
The main findings in summary are as follows:

- The model is able to reproduce the measured data
- The model is sufficiently general in nature to allow variations on the FCL design to be evaluated
- The modelling methodology developed should be applicable to a wide range of FCL designs

REFERENCES

[1] A. Hobl, S. Krämer, S. Elschner, C. Jänke, J. Bock and J. Schramm, "Superconducting fault current limiters — A new tool for the “Grid of the future”," Integration of Renewables into the Distribution Grid, CIRED 2012 Workshop, Lisbon, 2012, pp. 1-4.

[2] C. Waller, “Superconducting Fault Current Limiters,” Proc. Cryogenic Cluster Day Programme Sept. 28, 2011. [Online.] Available: http://www.stfc.ac.uk Accessed on 10 Sept. 2015.

[3] A. Morandi, "Fault Current Limiter: An Enabler for Increasing Safety and Power Quality of Distribution Networks," in IEEE Transactions on Applied Superconductivity, vol. 23, no. 6, pp. 5604608-5604608, Dec. 2013.

[4] B. P. Raju, K. C. Parton, T. C. Bartram, “A current limiting device using superconducting d.c. bias - applications and prospects,” *IEEE Trans Power Ap Syst*, vol. PAS-101, pp. 3173- 3177, 1982.

[5] Y. Xin, W. Gong, X. Niu, Z. Cao, J. Zhang, B. Tian, *et al.*, “Development of saturated iron core HTS fault current limiters,” *IEEE Trans Appl Supercond*, Vol. 17 (2), pp. 1760-1763, 2007.

[6] J. Moscrop, F. Darmann, “Design and development of a 3-phase saturated core high temperature superconducting fault current limiter,” Proc. Int. Conf. on Electric Power and Energy Conversion Systems, EPECS '09, Sharjah, 10-12 Nov. 2009, pp.1-6.

[7] F. Moriconi, F. De La Rosa, F. Darmann, A. Nelson, L. Masur, “Development and deployment of saturated-core fault current limiters in distribution and transmission substations,” *IEEE Trans Appl Supercond*, Vol. 21 (3), pp. 1288-1293, 2011.

[8] Y. Xin, W. Z. Gong, H. Hong, Y. Q. Gao, X. Y. Niu, J. Y. Zhang, *et al.*, “Development of a 220 kV/300 MVA superconductive fault current limiter,” *Supercond Sci Technol*, vol. 25, 2012. Paper ID: 105011.

[9] Y. Xin, W. Z. Gong, H. Hong, X. Y. Niu, J. Y. Zhang, A. R. Ren, B. Tian, “Saturated iron-core superconductive fault current limiter developed at Innopower,” AIP Conf. Proc. 1573, pp. 1042- 1048, 2014.

[10] H. Hong, Z. Cao, J. Zhang, X. Hu, J. Wang, X. Niu, *et al.*, “DC magnetization system for a 35 kV/90 MVA superconducting saturated iron-core fault current limiter,” *IEEE Trans Appl Supercond*, vol. 19 (3), pp. 1851-1854, 2009.

[11] D. Klaus, A. Morandi et al., "Development of a Saturated Core Fault Current Limiter With Open Magnetic Cores and Magnesium Diboride Saturating Coils," IEEE Transactions on Applied Superconductivity, Volume: 27 Issue: 4, Jun. 2017.